Oligomeric Assembly of Native-like Precursors Precedes Amyloid Formation by β-2 Microglobulin†

Catherine M. Eakin, Frank J. Attenello, Charles J. Morgan,‡ and Andrew D. Miranker*

Department of Molecular Biophysics and Biochemistry Yale University, 260 Whitney Avenue, New Haven, Connecticut 06520-8114

Received January 29, 2004; Revised Manuscript Received March 19, 2004

ABSTRACT: The deposition of β-2-microglobulin (β2m) as amyloid fibers results in debilitating complications for renal failure patients who are treated by hemodialysis. In vitro, wild-type β2m can be converted to amyloid under physiological conditions by exposure to biomedically relevant concentrations of Cu^{2+}. In this work, we have made comparative measurements of the structural and oligomeric changes in β2m at time points preceding fibrillogenesis. Our results show Cu^{2+} mediates the formation of a monomeric, activated state followed by the formation of a discrete dimeric intermediate. The dimeric intermediates then assemble into tetra- and hexameric forms which display little additional oligomerization on the time scales of their own formation (<1 h). Amyloid fiber formation progresses from these intermediate states but on much longer time scales (>1 week). Although Cu^{2+} is necessary for the generation and stabilization of these intermediates, it is not required for the stability of mature amyloid fibers. This suggests that Cu^{2+} acts as an initiating factor of amyloidosis by inducing oligomer formation. ^{1}H NMR and near-UV circular dichroism are used to establish that oligomeric intermediates are native-like in structure. The native-like structure and discrete oligomeric size of β2m amyloid intermediates suggest that this protein forms fibrils by structural domain swapping.

Amyloid fibers are highly ordered protein assemblies associated with an increasing number (>20) of human diseases, including Alzheimer's, type II diabetes, and dialysis related amyloidosis (DRA) (*1*). For each disease a different, normally soluble, protein precursor self-assembles into a fibrillar deposit. Despite differences in sequence and tertiary structure of the precursor proteins, amyloid fibers all share common features. These include, for example, a cross β-structure, where β-strands are arranged orthogonally to the fiber axis (*2*), and nucleation-dependent formation kinetics (*3*). The paradigm for understanding any chemical reaction is the identification of intermediate and transition states on the reaction pathway. This is essential for fibrillogenesis as the intermediates and not the mature fibers are likely responsible for cytotoxicity (*4*). It is therefore of fundamental and biomedical importance to understand how seemingly unrelated proteins can adopt a common amyloid structure.

DRA is a complication of long-term hemodialysis in which β2m accumulates as amyloid fibers in the bones and joints, resulting in a variety of destructive arthropathies (*5*). β2m is the 12-kDa polypeptide subunit necessary for the cell-surface expression of the class-I major histocompatibility complex (MHC) (*6*). In healthy individuals, β2m is released from the MHC and catabolized by the kidney. Upon kidney failure, however, β2m is not efficiently cleared from the serum. This results in the circulating concentrations of β2m increasing ∼10 times above the normal level of 0.1 μM. However, elevated concentrations of β2m are not unique to renal disease (*7*, *8*). Conversion of β2m to amyloid fibers must therefore be related to factors uniquely associated with hemodialysis therapy.

An analysis of physiological conditions relevant to uremic patients led to our discovery that β2m is a Cu^{2+} binding protein. Cu^{2+} binding by native and non-native states of β2m gives rise to destabilization and fiber formation at pH 7, 150 mM potassium acetate, and 37 °C (*9*, *10*). An increasing number of amyloid systems have also been shown to interact with divalent metal, particularly Cu^{2+}. These include prion protein from Creutzfeldt-Jakob disease (*11*, *12*), Aβ from Alzheimer's (*13*), α-synuclein from Parkinson's (*14*), and immunoglobulin light chains from light chain amyloidosis (*15*). This suggests that divalent metal interactions may represent a motif in inducing amyloidogenic structures. The mechanism of Cu^{2+} associated amyloid formation is, however, largely unknown. In this work, we have made comparative measurements of the structural and oligomeric changes in β2m at time points preceding amyloid formation. Through the use of NMR, circular dichroism (CD), fluorescence, and analytical ultracentrifugation, we have identified and characterized obligate intermediates formed during fibrillogenesis.

† This work was supported by the NIH (DK54899) and the Pew charitable trusts (PO219SC).

* To whom correspondence should be addressed. Voice: (203) 432−8954. Fax: (203) 432-5175. E-mail: Andrew.Miranker@yale.edu.

‡ Present address: Genzyme Corporation, 1 Mountain Road, Framingham, MA 01701.

[1] Abbreviations: β2m, β-2 microglobulin; $β2m_{Cu}$, β-2 microglobulin in the presence of Cu^{2+}; CD; circular dichroism; DRA, dialysis related amyloidosis; EM, electron microscopy; MW, molecular weight; NMR, nuclear magnetic resonance spectroscopy; PFG, pulse field gradient; SV, sedimentation velocity analytical ultracentrifugation; ThT, thioflavin T.

10.1021/bi049792q CCC: $27.50
Published on Web 05/26/2004

MATERIALS AND METHODS

Chemicals. Buffers and salts were obtained from Sigma-Aldrich (Milwaukee, WI) or J. T. Baker (Phillipsburg, NJ), and cell culture media from Becton Dickinson (Sparks, MD).

Protein Isolation. Human β2m was expressed in *Escherichia coli* (*10*). BL21(DE3) cells transformed with pHN1-β2m were grown at 37 °C to an OD at 600 nm of 0.6, then induced with 500 μM IPTG for 2 h. Protein was solubilized from inclusion bodies using 8 M urea, 100 mM tris, 100 mM EDTA, and 10 mM methionine, pH 7.4 and oxidatively refolded by dilution into the absence of urea. Protein was concentrated by tangential flow (Vivascience (Hannover, Germany) vivaflow 50, 5 kDa cutoff). Contaminates were then removed by size exclusion chromatography (Superdex 75). Purity of ≥95% was assessed by SDS−PAGE. The oxidation state of the disulfide bond in β2m between C25 and C80 was assessed as described previously (*10*). Only protein with <10% reduced material was used. Human derived β2m was purified from the urine of Dent's disease patients (*9*). Urine was filtered (0.2 μm) and cut with 2.1 M ammonium sulfate. Insoluble material was removed by centrifugation, and the soluble fraction cut again with an additional 1.0 M ammonium sulfate. Precipitate was resuspended and applied directly to a Cu^{2+} charged NTA-Superflow (Qiagen, Germany), washed (3×) with 5 mM potassium phosphate, 10 mM KCl, 1 mM imidazole, 10 mM methionine, pH 7.4, and eluted (5×) with 10 mM imidazole. β2m containing fractions were pooled, concentrated, and further purified by size exclusion chromatography.

Amyloid Formation. β2m fibers were formed by incubating 100 μM β2m, 200 μM Cu^{2+}, 25 mM MOPS, 200 mM $KC_2H_3O_2$, 500 mM urea, pH 7.4 in quartz cuvettes at 37 °C. All components were equilibrated at 37 °C prior to Cu^{2+} addition, and immediately returned to 37 °C after mixing ($t = 0$). Control samples contained 10 mM EDTA and no Cu^{2+}. Real-time measurements were performed either by ^{1}H NMR, or by fluorescence using 80 μM thioflavin T (*16*). Dead times of measurement were ∼10 min and ∼30 s, respectively.

Electron Microscopy. Solutions containing amyloid were centrifuged (14000*g*, 10 min), and the pellet was resuspended in 10 μL of the supernatant. Samples were applied to carbon-coated copper grids prepared in-house. Grids were stained with 1% phosphotungstic acid for 30 s. Images were collected using a Phillips Technai 12 operating at 120 kV, using a 1024 × 1024 pixel Gatan 794 slow scan CCD in underfocus.

Analytical Ultracentrifugation. Sedimentation velocity at 40 000 rpm and 20 °C was performed with human derived β2m ∼20 h after the addition of Cu^{2+} using a Beckman XL-A analytical ultracentrifuge. Radial scans were acquired at 295 nm for ∼10 h. Data analysis was performed assuming a spherical shape using the continuous c(s) distribution model, independent species model, and confidence interval in M feature in SedFit v8.5 (*17*).

NMR. NMR spectra were recorded in-house using a 500 MHz Varian Unity Inova. 1D spectra were collected using field gradient based water suppression (*18*), sweep width of 8000 Hz, collecting 8192 points and 400 transients. A 6 s relaxation delay was used for quantitation in which protein intensity was renormalized to the trimethylsilylpropionate (TMSP) internal standard. Real-time measurements were collected with 100 transients at a 1.2 s relaxation delay, repeated for ∼1.5 h. The presence of 500 mM urea was included in all NMR samples to match conditions of fiber reactions; this allows only the upfield regions to be used for analysis. Diffusion was measured and analyzed as per ref *19*, collecting 8192 points and 2016 transients between gradient strengths of 5 and 23 G/cm. Gradients were calibrated using the residual water peak in 99.9% D_2O. Molecular weights were calculated using Stokes law and assuming a spherical shape. NMR data was processed using Vnmr, and SpinWorks (Kirk Marat, University of Manitoba). The apo sample was 100 μM β2m, 10% D_2O, 200 mM $NaC_2H_3O_2$-d_3, 500 mM urea, pH 7.4, 37 °C. The β2m + Cu^{2+} and β2m + Zn^{2+} samples were collected under the same conditions as apo samples, but contained 200 μM $CuCl_2$ or 300 μM $ZnCl_2$, respectively.

Circular Dichroism (CD). CD experiments were performed on an Aviv model 215 spectrometer. Near-UV spectra (330−240 nm) were collected in a 3-mm path-length cell with 100 μM β2m, 25 mM MOPS, 200 mM $KC_2H_3O_2$, 500 mM urea, pH 7.4, 37 °C. $\beta2m_{Cu}$ contained 200 μM $Cu(C_2H_3O_2)_2$. Only near-UV CD is shown as MOPS was included for consistency with other experiments and MOPS absorbs in the far-UV.

Fluorescence. Fluorescence measurements were made using a PTI Quantamaster C-61 with 4-nm slit widths. For kinetic experiments monitoring ThT fluorescence enhancement, monochromators were set to 440 and 492 nm for excitation and emission, respectively. Excitation scans were corrected for lamp intensity and monitored from 300 to 470 nm with emission at 492 nm.

Calculations and Fitting. All curve fitting and calculations in this work were performed using the NonlinearRegress function in Mathematica 4.2 (Wolfram Research Inc., Champaign IL). All experiments represented in this work were repeated ≥3 times, with errors reported as ± one SEM.

RESULTS

The conversion of soluble β2m into amyloid fibers will involve structural as well as oligomeric changes. To monitor these changes, we have designed and conducted a series of experiments to identify intermediates during amyloid formation. We first established a standard fibrillogenesis reaction with an extended time scale to allow investigation and analysis of components during amyloid assembly. Oligomeric changes in β2m during assembly were detected by physical approaches including nuclear magnetic resonance (NMR), analytical ultracentrifugation, and fluorescence. Finally, structural changes during amyloid formation were assessed directly using optical and NMR spectroscopies, and indirectly using reaction kinetics.

In uremic patients, β2m amyloid forms over a period of years (*5*). In vitro, incubation for 1−2 weeks of 100 μM β2m in 200 μM $Cu(C_2H_3O_2)_2$, 25 mM MOPS, 200 mM $KC_2H_3O_2$, 500 mM urea, pH 7.4, 37 °C, and no stirring, results in conversion of ∼50% of the protein into a pelletable form. Amyloid fibers are readily apparent in suspensions of these pellets (Figure 1A). Unless otherwise stated, the above conditions represent our standard reaction used in all assays.

Cu^{2+} associated β2m amyloid formation occurs under conditions in which the apparent stability of β2m is unaffected by the presence of Cu^{2+}. Our previous assessments

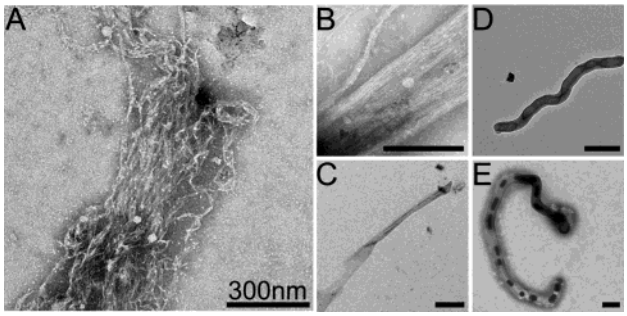

FIGURE 1: Transmission electron micrograph images of β2m amyloid fibers formed after ~2 weeks at 37 °C in the presence of 100 μM β2m and 200 μM Cu^{2+}. The majority of aggregates observed are filamentous (A, B). Tapes (C), and tubular (D, E) structures are also observed within the same samples. All scale bars are 300 nm.

of β2m stability in the presence of Cu^{2+} were made at a 36:1 Cu^{2+}:β2m ratio (*9*). At the 2:1 Cu^{2+}:β2m ratio used here to form amyloid fibers, the apparent stability measured by urea denaturation of β2m is 28 kJ/mol (not shown). This is comparable to our reported stability in the absence of metal (33 kJ/mol) (*9*, *10*). The vast majority of aggregates detected by EM are fibrous (Figure 1A). However, large mats of aligned fibers (Figure 1B), tapes (Figure 1C), and large tubular structures (Figure 1D,E) are also observed. Interestingly, these distinct types of aggregation are all formed in the same sample and are not observed in samples incubated with EDTA (not shown). Thus, Cu^{2+} is required to initiate aggregation and acts on conformational states that do not contribute to the global stability.

Intermediates of Cu^{2+} associated β2m amyloid formation were detected by NMR diffusion measurements using pulsed field gradients (PFG) (*19*, *20*). Diffusion constants of β2m were assessed in the presence and absence of Cu^{2+} over the first ~20 h of incubation. The diffusion constant of β2m is $1.5 \pm 0.1 \times 10^{-6}$ cm^2/s in the absence, and $1.2 \pm 0.1 \times 10^{-6}$ cm^2/s in the presence of Cu^{2+} (Figure 2A). For apo-β2m, this yields an apparent molecular weight (MW) of 17 $\pm$ 4 kDa, which is in reasonable agreement with the monomeric MW of 11.9 kDa. The larger apparent MW may be attributed, in part, to a hydration layer surrounding the protein. In contrast, β2m in the presence of Cu^{2+} ($\beta 2m_{Cu}$) gives an apparent MW of 39 $\pm$ 8 kDa. The confidence interval and spherical assumption, however, preclude an exact MW determination for the copper induced species. Nevertheless, the PFG diffusion measurement plainly indicates that $\beta 2m_{Cu}$ is affected by the sampling of oligomeric states.

A precise determination of the species formed by $\beta 2m_{Cu}$ was elucidated using sedimentation velocity (SV) analytical ultracentrifugation. Intriguingly, SV reveals three discrete populations following incubation of β2m with Cu^{2+}, but only one population in the absence of Cu^{2+} (Figure 2B). In the presence of Cu^{2+} the first population has a Svedberg (S) value of 1.3 giving an apparent MW of 13.5 $\pm$ 0.8 kDa. This is similar to 11.8 $\pm$ 0.1 kDa determined for the monomeric apo-β2m control (Figure 2B). The second population (2.9S) has an apparent MW of 26.6 $\pm$ 3.5 kDa, which is within error of dimeric β2m. The apparent MW of the third population (4.9S) is 55.7 $\pm$ 5.5 kDa. This is too large to be attributed to trimeric β2m, indicating that trimeric β2m is not observed (Figure 2B, inset). In repeat experiments, the confidence interval of 4.9S extends to MWs as high as ~80 kDa (not shown). This suggests this peak may represent multiple species, such as a combination of tetrameric (46.8 kDa) and hexameric (70.2 kDa) β2m. The presence of discrete dimer and the absence of trimeric β2m implies larger oligomeric states are built from dimeric rather than monomeric units. Furthermore, the discrete nature of the peaks indicates that oligomer interconversions are slow compared to the time of SV analysis (~10 h), and that oligomer assembly occurs prior to centrifugation (~20 h).

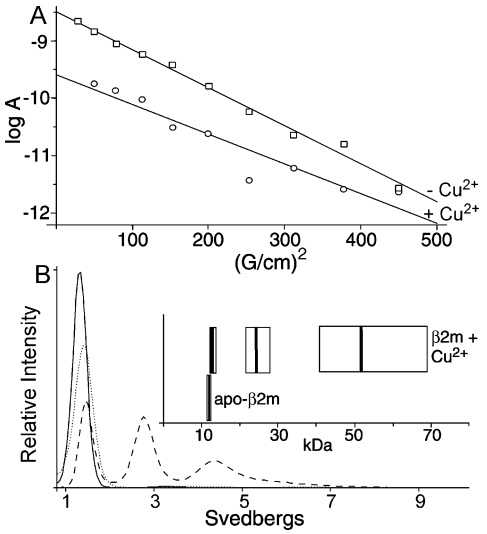

FIGURE 2: Oligomeric states of β2m in the presence of Cu^{2+} are detected by PFG diffusion (A) and SV (B). (A) Representative plot of 100 μM β2m PFG diffusion measurements in the presence (○) and absence of 200 μM Cu^{2+} (□). (B) SV was performed with 86 μM β2m in the absence (solid) or presence of 200 μM Cu^{2+} (dash), and after addition of 10 mM EDTA to the latter (dots). A representative maximum entropy fit of these samples is shown. Subsequent fitting with discrete noninteracting species yielded molecular weight values shown as bold lines in inset.

The oligomeric intermediates are amyloid-like as evident by binding of the histological dye, thioflavin T (ThT). ThT is a fluorescent dye commonly used to distinguish amyloid fibers from native protein and amorphous aggregates. Binding to the ordered environment of the fiber results in a characteristic excitation shift of 120 nm (Figure 3A) (*16*). Under conditions used to monitor oligomer formation by NMR and SV, β2m gives rise to this characteristic shift (Figure 3A). This enables kinetic measurements to be made on the minute time scale. To determine the rate of intermediate formation, β2m was mixed with Cu^{2+} in the presence of ThT and monitored over ~24 h. During the first hour, ThT fluorescence increases exponentially giving an apparent rate of $1.6 \pm 0.04 \times 10^{-3}$ s^{-1} (Figure 3B). Although a ThT fluorescence enhancement is observed after an hour, no fibers, protofibrils, or aggregates are detectable by EM from these samples (not shown). This suggests that oligomers and full-length fibers bind ThT in a similar manner. Furthermore, incubation on the amyloid forming time scale (~week) fails to significantly change the ThT signal. This indicates that the ThT signal at 1 h is not from a subpopulation of amyloid, and that a similar structure may exist between the oligomers and amyloid fibers. Importantly, ThT itself is not causal to this observation as experiments in which a reaction is aliquoted at discrete times prior to ThT exposure yields the same kinetic profile (not shown). Thus, from ThT fluores-

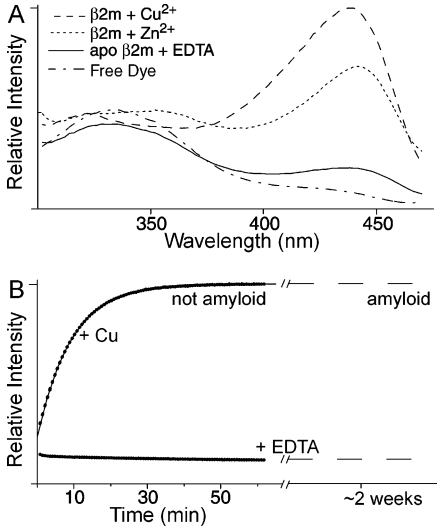

FIGURE 3: β2m oligomers formed in the presence of Cu^{2+} show ThT fluorescence enhancement. (A) ThT excitation of free dye, and 100 μM β2m in the presence and absence of 200 μM Cu^{2+} or 300 μM Zn^{2+}. Intensities are renormalized from the blank ThT peak at 340 nm. (B) Fluorescence enhancement kinetics of 100 μM β2m in the presence and absence of 200 μM Cu^{2+} at 37 °C. In the presence of Cu^{2+}, the increase in ThT fluorescence enhancement is $1.6 \pm 0.04 \times 10^{-3}$ s^{-1}. No change is detected in the presence of EDTA. The ThT signal of $\beta 2m_{Cu}$ does not significantly change over several weeks (B, dashed line for illustration purposes).

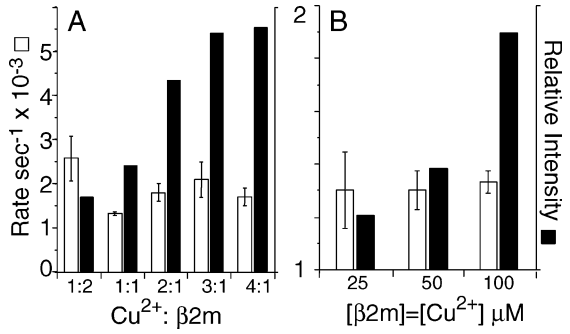

FIGURE 4: Changes in the ratio of Cu^{2+}:β2m (A) and in the concentration of β2m (B) do not affect the rate of oligomer formation. (A) The proportion of Cu^{2+}:β2m was varied from 1:2 to 4:1 at a fixed β2m concentration of 50 μM. No change in rate of oligomer formation was observed (A, □). The amount of oligomer formed is estimated by the ThT excitation signal at 440 nm (A, ■). (B) Changes in the concentration of β2m from 100 to 25 μM, at a constant Cu^{2+}:β2m ratio of 1:1, does not affect the rate of oligomer formation (B, □). Higher protein concentrations form more oligomer as determined by ThT excitation signal at 440 nm (B, ■). Below 25 μM β2m the signal-to-noise ratio is significantly diminished, inhibiting accurate measurements.

cence enhancement, oligomer formation is apparently complete on a 1-h time scale.

Divalent copper is an essential part of the oligomeric structure of the intermediates, but not of mature β2m amyloid. Varying the ratio of Cu^{2+}:β2m from 1:2 to 4:1, results in no change in the rate of intermediate formation (Figure 4A, open bars). This suggests that Cu^{2+} binding is not rate-limiting in the formation of intermediates. By contrast, the total ThT signal shows a dose dependent increase with Cu^{2+} concentration, which appears to saturate at a ratio of 3:1 (Figure 4A, closed bars). β2m oligomers formed after 1 h fully revert to monomer after EDTA addition. This is apparent by SV (Figure 2B), NMR (not

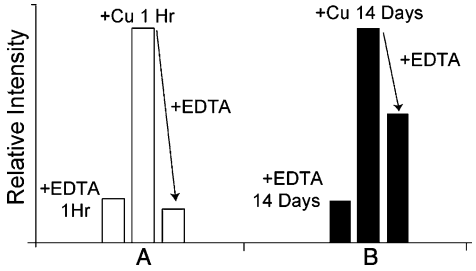

FIGURE 5: Sensitivity of ThT fluorescence enhancement to EDTA. (A, □) Addition of EDTA to $\beta 2m_{Cu}$ after 1 h of incubation completely reverses the ThT fluorescence enhancement to that of apo-β2m. The ThT signal does not recover even after weeks of incubation (not shown). (B, ■) Addition of EDTA to $\beta 2m_{Cu}$ samples incubated for 14 days does not significantly affect the ThT fluorescence enhancement. Extended incubation of these samples ($\sim$ week) after EDTA addition does not diminish the ThT fluorescence enhancement (not shown).

shown), and ThT fluorescence (Figure 5A). By contrast, incubation for two weeks results in amyloid and ThT fluorescence, which is no longer fully reversible by the addition of EDTA (Figure 5B). Therefore, between 1 h and 2 weeks, Cu^{2+} induced oligomerization of β2m loses the energetic requirement for Cu^{2+}.

Oligomeric intermediates of β2m are structurally similar to native β2m. This is evident from the similar near-UV CD profiles of apo-β2m and $\beta 2m_{Cu}$ oligomers which display positive bands at 270 and 290 nm (Figure 6A). These bands arise from the packing of aromatic groups into a fixed and well-defined chiral environment. Therefore, these bands provide a characteristic fingerprint for native protein structures (*21*). Tertiary structural rearrangements accompanying β2m oligomerization are expected to cause significant differences in this region of the spectrum. The $\beta 2m_{Cu}$ intermediates and apo-β2m also have closely similar ^{1}H NMR spectra (Figure 6B,C). Most notably, both $\beta 2m_{Cu}$ and apo-β2m have ring shifted methyl protons at ~ -0.5 ppm which require a well-defined three-dimensional structure. Furthermore, no additional peaks are evident in $\beta 2m_{Cu}$ although several peaks have disappeared. Isolated peaks in $\beta 2m_{Cu}$ are broadened by $\sim$10 Hz relative to apo-β2m. For comparison, hen lysozyme peaks are broadened by $\sim$5 Hz under the same solution conditions (not shown). This indicates that peak broadening can only be attributed in part to paramagnetic effects of Cu^{2+}. To separate line broadening contributions of unpaired electrons from those derived from oligomerization, intermediates were also formed by the addition of diamagnetic Zn^{2+}. We have previously shown that β2m can bind and be destabilized by Zn^{2+}, although using >100-fold more Zn^{2+} than Cu^{2+} (*10*). Surprisingly, the addition of Zn^{2+} to β2m at a ratio of 3:1 results in oligomer formation by SV (not shown), and induces ThT fluorescent enhancement with a rate and amplitude comparable to 2:1 Cu^{2+}:β2m (Figure 3A). In the presence of Zn^{2+}, ^{1}H NMR spectra are identical to apo-β2m with respect to chemical shifts; however, peaks are broadened (Figure 6D). This suggests $\beta 2m_{Cu}$ oligomers have increased correlation times, but the structure remains similar to apo-β2m. In both analyses, the closely similar ^{1}H NMR and near-UV CD spectra are consistent with the maintenance of native structure by $\beta 2m_{Cu}$ oligomers.

Oligomerization is responsible for formation of amyloid-like ThT fluorescence enhancement. Oligomer formation was

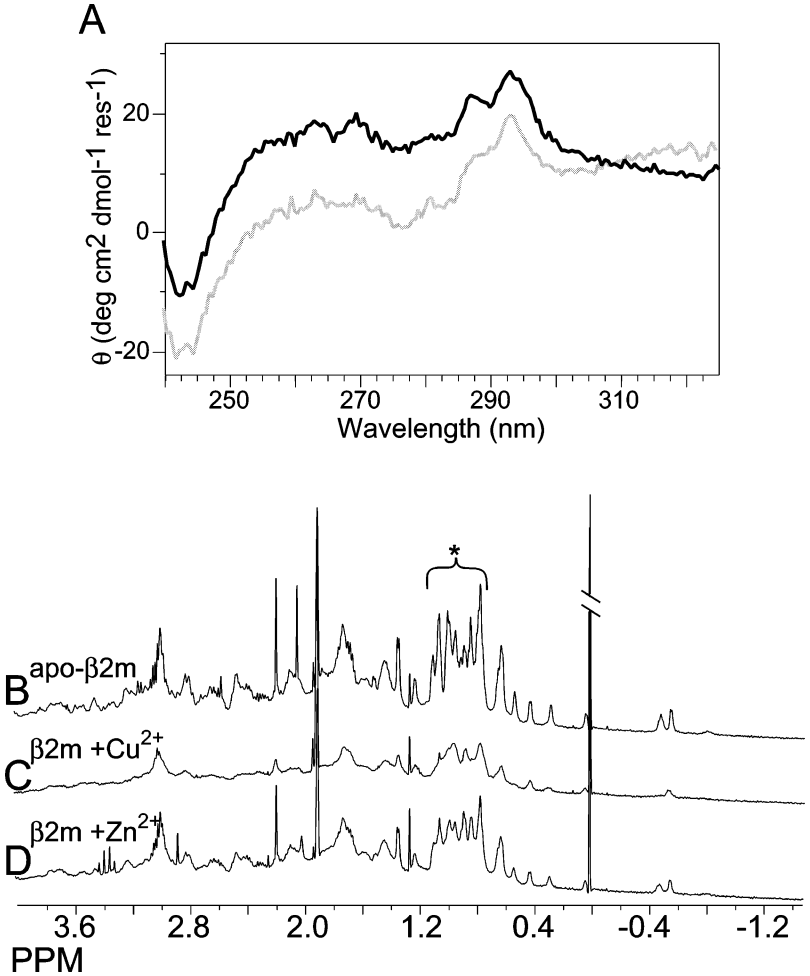

FIGURE 6: β2m oligomers are native-like in structure as determined by near-UV CD and ^{1}H NMR. Near-UV CD spectra of β2m in the presence and absence of Cu^{2+} are shown in (A). CD spectra are 100 μM β2m, 500 mM urea, 25 mM MOPS, 200 mM $KC_2H_3O_2$, 37 °C. Apo-β2m is shown in black, and $\beta 2m_{Cu}$ is in gray. NMR spectra between 3.8 and −1.4 ppm of β2m in the presence and absence of Cu^{2+} or Zn^{2+} are shown (B−D). All NMR spectra are 100 μM protein in the presence of 500 mM urea, 200 mM $Na(C_2H_3O_2)$-d_3, 10% D_2O, 100 μM TMSP, 37 °C, and are referenced to TMSP. (B) apo-β2m (C) $\beta 2m_{Cu}$ (D) β2m in the presence of Zn^{2+}. The (*) denotes a region where peak broadening differences are readily apparent.

additionally quantitated using ^{1}H signals normalized against an internal standard (TMSP). Relative to apo-β2m, 60% of the $\beta 2m_{Cu}$ NMR signal is lost (Figure 6B,C). By contrast, no signal loss is observed for lysozyme in the presence of Cu^{2+}. Cu^{2+} is a paramagnetic ion and can cause resonances near bound Cu^{2+} to relax during the 500 μs delay preceding data acquisition (*22*). Signal loss was therefore assessed for β2m incubated with Zn^{2+} (see above). Oligomer formation using Zn^{2+} similarly resulted in 40% ^{1}H signal loss (Figure 6D). This indicates that signal loss is the result of increased correlation times associated with oligomerization. The oligomerization process was assessed in real-time by measurement of ^{1}H NMR signal loss. ^{1}H signal loss is clearly observed to occur at a similar rate as ThT fluorescence enhancement (Figure 7). The loss of ^{1}H signal intensity of β2m in the presence of Cu^{2+} or Zn^{2+} (not shown) occurs at rate of $1.9 \pm 0.1 \times 10^{-3}$ and $3.3 \pm 0.4 \times 10^{-4}$ s^{-1}, respectively. These rates compare well with the gain in ThT fluorescence enhancement of $1.6 \pm 0.04 \times 10^{-3}$ and $8.0 \pm 1.2 \times 10^{-4}$ s^{-1}, respectively. After ~1 h in the presence of Cu^{2+} 35% of the β2m ^{1}H signal is lost. This loss in signal correlates well with the 40% signal loss observed in Zn^{2+} and the 25% of the β2m observed by SV in the 4.9S peak (Figure 2B). This suggests that the 4.9S peak includes species

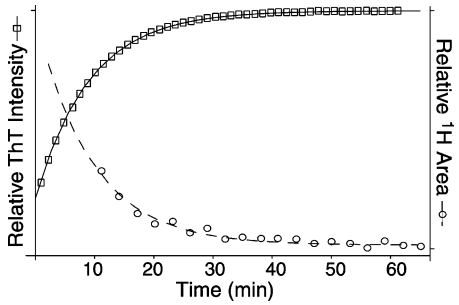

FIGURE 7: The formation of oligomers occurs with the same rate as the ThT fluorescence enhancement. $\beta 2m_{Cu}$ forms oligomers with a rate of $1.9 \pm 0.1 \times 10^{-3}$ s^{-1} as monitored by ^{1}H NMR signal loss (○) over time. Peaks were integrated between 1.12 and 0.7 ppm. This rate is similar to the rate of $1.6 \pm 0.04 \times 10^{-3}$ s^{-1} from the gain in ThT fluorescence enhancement (□).

which do not strongly contribute to the ^{1}H NMR signal. Further loss of ^{1}H signal continues for days at a much slower rate (not shown). The signal decrease over the first hour is therefore due to formation of oligomers $n > 4$, and subsequent loss likely derives from formation of larger oligomers and subsequent fibers.

The reaction order of the rate-limiting step for oligomer formation was assessed by measuring the concentration

dependence of the kinetics. Kinetic profiles of ThT enhancement were performed at three protein concentrations, 25, 50, and 100 μM, at a 1:1 Cu^{2+}:β2m ratio. The relative amount of intermediate formed scales in direct proportion to the protein concentration. This is consistent with Cu^{2+} acting as a constituent of the oligomeric structures. Surprisingly, the rate of fluorescence enhancement is not significantly affected by changes in protein concentration (Figure 4B). This suggests the ThT fluorescence enhancement in the presence of Cu^{2+} is rate limited by a conformational rearrangement.

DISCUSSION

Identifying and characterizing intermediates is central to understanding the mechanism of fibril assembly and toxicity in amyloid diseases. Here, we have performed a series of experiments that reveal intermediates of amyloid formation by β2m. Seven key observations contribute strongly to our structural and energetic understanding of this system: (i) Cu^{2+}-induced amyloid formation does not require global destabilization of β2m. (ii) $\beta 2m_{Cu}$ forms amyloid with a 1 week to 1 month time constant under near-physiological conditions. (iii) Intermediate conformations and oligomers are formed with 1 h time constants. (iv) The rate of intermediate formation is insensitive to Cu^{2+} and protein concentrations. (v) Rapidly formed intermediates but not mature amyloid require Cu^{2+} for stability. (vi) Intermediate oligomers assemble with discrete, dimeric additions. (vii) Intermediates are native-like in structure.

In the presence of Cu^{2+}, a monomeric activated state of β2m is formed (M^*). This is a direct consequence of our observation that oligomer formation kinetics are insensitive to protein concentration (Figure 4B). Concentration independence may result from either a rate-limiting unimolecular step which precedes oligomerization, or a conformational change which occurs after assembly has taken place. A preceding step is more likely since oligomerization detected by ThT fluorescence enhancement is correlated to oligomerization detected by ^{1}H signal loss (Figure 7). As β2m is not globally destabilized by the levels of Cu^{2+} used here, the formation of β2m oligomers likely derives from copper bound native β2m ($M{\cdot}Cu^{2+}$). Cu^{2+} binding is not, however, the rate limiting step since we have previously shown Cu^{2+} binding to native β2m occurs in the dead time ($\sim$1 min) of assessment (*9*, *10*). Here, we also observe that fluorescent enhancement kinetics are insensitive to Cu^{2+} concentration (Figure 4A). This indicates that the rate-limiting step to oligomer formation is mediated by a copper bound state. Rapid formation ($<$1 min) of $M{\cdot}Cu^{2+}$ is therefore followed by slow ($\sim$1 h) transition to an activated state, M*, which subsequently gives rise to oligomeric assembly.

During amyloid formation, oligomeric intermediates build to a critical size, I^n, which no longer requires Cu^{2+} for stability. The observation of dimer (I^2), but not trimer by SV, suggests that I^2 is the building unit of higher order oligomers (Figure 2B inset). Furthermore, oligomeric assembly occurs on a faster time scale (Figure 7) than the formation of M* (1.6×10^{-3} s^{-1}). However, the oligomers of $n \leq 6$ continue to dominate the solution for at least $\sim$30 h as measured by SV (Figure 2B). This suggests oligomeric assembly is Cu^{2+} dependent since consumption of Cu^{2+}

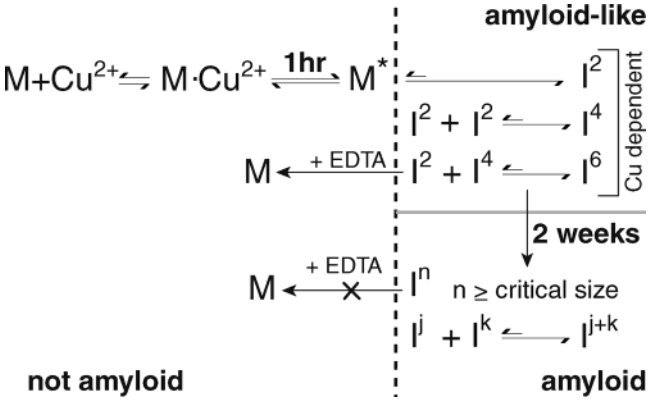

FIGURE 8: Model for β2m amyloid formation. M is native β2m, $M{\cdot}Cu^{2+}$ is Cu^{2+} bound native state β2m, M* is activated protein. I^2, I^4, I^6 are di-, tetra-, and hexameric β2m, respectively. Formation of these oligomers is dependent on Cu^{2+}. Oligomers of critical size I^n are no longer sensitive to the addition of EDTA. Further oligomerization after forming a critical size is generically represented by assuming annealing of oligomers of size *j* and *k*. The dotted line delineates states with enhanced ThT fluorescence as fibers and oligomeric intermediates (right side), from ThT negative states such as native β2m, M (left side). The gray line delineates conversion of prefibrillar oligomeric intermediates to amyloid fibers.

would result in an eventual slowing of oligomer formation. It is tempting to further use this construct to reconcile the $\sim$1 h formation of intermediates with the $\sim$2 week time scale of amyloid formation. However, oligomeric intermediates are fully reversed by addition of EDTA while fibers are not (Figure 5). This suggests that in the formation of oligomeric intermediates, a critical size of I^n ($n \geq 6$) is reached (*3*), where the free energy of intermolecular contacts exceeds that provided by Cu^{2+}. In addition, this result indicates that in vivo levels of Cu^{2+} are irrelevant to the stability of β2m fibril deposits. Rather, Cu^{2+} is only required for fiber nucleation, the probable site of which is contact with dialysate (*9*, *23*).

A minimal model that summarizes our results and assertions is shown in Figure 8. In this model, native β2m (M) binds Cu^{2+} ($M{\cdot}Cu^{2+}$) and over 1 h forms the M^* activated state. Di-, tetra-, and hexameric (I^2, I^4, and I^6) oligomers are formed following the conversion to M^*. The formation of these oligomers is fast relative to the formation of M^* and is Cu^{2+} dependent (see above). The assembly of oligomers occurs in discrete units of two. Upon reaching a critical size, I^n, oligomers are no longer sensitive to EDTA addition. Fiber elongation is generically represented by assuming annealing of oligomers of size *j* and *k*. Oligomer annealing, as for repolymerization of actin (*24*) and microtubules (*25*) after shearing, requires the diffusional encounter of two oligomers. Since the molar concentration of oligomers decreases as the size of oligomers increases, oligomer annealing slows over time. In the case of β2m, we conjecture that this process contributes to the slow formation of amyloid from oligomers.

The oligomeric intermediates have native-like conformation. This is most clearly observed in their native-like ^{1}H NMR spectra and near-UV CD signal (Figure 6). The effect of chemical exchange on apparent ^{1}H intensities must be negligible, since interconversion is slow on the SV time scale (hours). This indicates the ^{1}H and CD spectra observed after $>$1 h Cu^{2+} incubation are a sum of spectra from each of the states observed by SV. Oligomeric assembly of $\beta 2m_{Cu}$ is also observed in ^{1}H spectra as an apparent signal loss, due

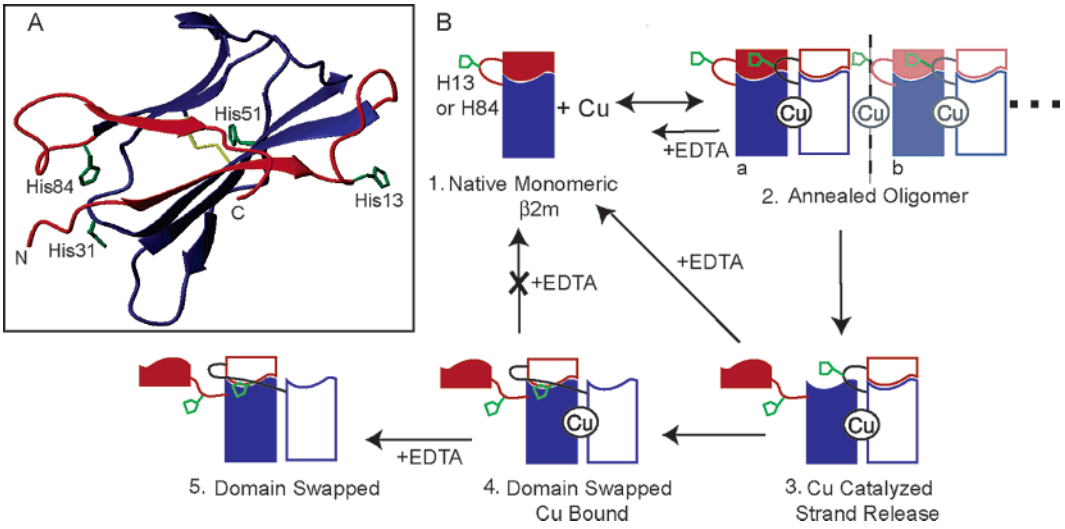

FIGURE 9: (A) Structure of β2m (2CLR) showing all histidine (green) and cystine (yellow) residues. The N- and C-terminal strands are shown in red. His13 is on the loop following the N-terminal strand and His84 is on the loop prior to the C-terminal strand. (B) Schematic of the suggested model for β2m domain swapped oligomers. Native monomeric β2m (1) binds Cu^{2+} at His31 and forms annealed oligomers (2a). Cu^{2+}-dependent annealing of oligomers continues in discrete units of two (2b). Interactions of His13 or His84 with Cu^{2+} catalyze the release of a terminal strand to initiate domain swapping (3). Promotion of strand release could occur by His13 or His84 interacting with Cu^{2+} bound at the native binding site (His31) or from interactions with additional Cu^{2+}. Following strand release, domain swapped structures are formed (4). Annealed oligomers (2) and oligomers with a released strand (3) are reversed to monomeric β2m upon the addition of EDTA, i.e., Cu^{2+} is required for stabilization of these states. Domain swapped structures, however, are stable even after chelation of Cu^{2+} ions (5).

to increased correlation times of larger species (Figure 7). ^{1}H spectra are, therefore, dominated by contributions from monomeric and dimeric β2m, the latter of which is ~45% of the population by SV. Tetra- and hexameric β2m will also contribute to the ^{1}H spectra but with diminished apparent intensity. Thus, while oligomers of β2m are necessarily contributing to observed ^{1}H NMR spectra, they are indistinguishable from native state β2m.

The presence of oligomers whose subunits have native-like structure suggests that the mechanism of β2m fiber formation is either through subunit annealing, or domain swapping. The domain swap model is based on studies of intertwined dimers observed crystallographically (*26*). This model postulates that a chain can be formed by each monomer swapping a strand or subdomain into the same environment of an identical monomer (*27*−*29*). Evidence of domain swapping as a mechanism of amyloid formation has been observed in prion protein (*30*) and cystatin C (*31*, *32*). In addition, domain swapping has previously been proposed as a mechanism for β2m amyloid formation (*33*). Several observations reported here are consistent with these mechanisms. These include: (1) Amyloid and intermediates are formed without the requirement for significant destabilization of the protein. (2) Oligomeric intermediates are composed of domains with native-like structure. (3) ThT fluorescence enhancement of β2m amyloid is closely similar to that of its amyloidogenic intermediates. In addition, we report a time-dependent rearrangement in which oligomers become resistant to dissociation with EDTA (Figure 5). Taken together, these observations suggest the mechanism of β2m amyloid formation is structural domain swapping.

No consensus sequence has been identified among the ~40 proteins with domain swapped structures. However, in most cases the swapped domain is located at a terminus (*26*). In β2m, copper is likely coordinated by histidine residues. β2m has histidine residues located on the loops prior to both the N- (His13), and C- (His84) terminal β-strands (Figure 9A). In addition, both of these residues have previously been shown to coordinate Cu^{2+} in non-native states (*10*). These strands also have been implicated in protecting monomeric β2m from fibril formation (*33*−*35*). Loss of native contact with these strands causes loss of the edge strand protective features and can promote aggregation. Further, destabilization of these strands through specific point mutations has caused β2m to form amyloid fibers at neutral pH (*33*). The release at the C- or N-terminus as a single strand is also structurally favorable since the C25−C80 disulfide bond tethers the adjacent stands. Therefore, we conjecture that copper coordination by β2m at His13 or His84 induces structural rearrangements of the protein, which frees either the N- or C-terminus, allowing the formation of a domain swapped structure (Figure 9B). Once such a structure is formed, the requirement for Cu^{2+} is lost.

The oligomeric species characterized here are particularly important in determining the structural and dynamic properties of β2m in DRA. In addition, the general importance of divalent cations affecting protein conformations is considerably more widespread. For example, Zn^{2+} productively mediates a variety of structures through bridging of cystine thiols, as for example in Zn^{2+} finger proteins (*36*). Pathologically, Cu^{2+} plays a structural role in other amyloid diseases including Creutzfeldt-Jakob (*11*), Alzheimer's (*37*), Parkinson's (*14*), and light chain amyloidosis (*15*). In addition, Cu^{2+} has been shown to induce structure in natively unfolded α-synuclein from Parkinson's disease (*14*), and the N-terminal unstructured region of prion protein from Creutzfeldt-Jakob disease (*38*, *39*). Determining the mechanism of Cu^{2+}-mediated oligomeric assembly is therefore important to a wider understanding of amyloid assembly. For β2m in particular, structural characterization of oligomeric intermediates should allow for the development of therapeutic strategies against DRA.

ACKNOWLEDGMENT

We thank Dr. S. Jaswal for helpful discussions, Professor V. Unger for assistance with electron microscopy, and Professors L. Regan and A. Hamilton for use of CD spectrophotometer. We also thank Erin Matthews for assistance with SV, and Professor D. Engelman for use of analytical ultracentrifuge.

REFERENCES

1. Rochet, J. C., and Lansbury, P. T., Jr. (2000) Amyloid fibrillogenesis: themes and variations, *Curr. Opin. Struct. Biol. 10*, 60−68.
2. Sunde, M., Serpell, L. C., Bartlam, M., Fraser, P. E., Pepys, M. B., and Blake, C. C. (1997) Common core structure of amyloid fibrils by synchrotron X-ray diffraction, *J. Mol. Biol. 273*, 729−739.
3. Harper, J. D., and Lansbury, P. T., Jr. (1997) Models of amyloid seeding in Alzheimer's disease and scrapie: mechanistic truths and physiological consequences of the time-dependent solubility of amyloid proteins, *Annu. Rev. Biochem. 66*, 385−407.
4. Hardy, J., and Selkoe, D. J. (2002) The amyloid hypothesis of Alzheimer's disease: progress and problems on the road to therapeutics, *Science 297*, 353−356.
5. Floege, J., and Ehlerding, G. (1996) Beta-2-microglobulin-associated amyloidosis, *Nephron 72*, 9−26.
6. Bjorkman, P. J., Saper, M. A., Samraoui, B., Bennett, W. S., Strominger, J. L., and Wiley, D. C. (1987) Structure Of the Human Class-I Histocompatibility Antigen, Hla-A2, *Nature 329*, 506−512.
7. Malaguarnera, M., Restuccia, S., Di Fazio, I., Zoccolo, A. M., Trovato, B. A., and Pistone, G. (1997) Serum beta2-microglobulin in chronic hepatitis C, *Dig. Dis. Sci. 42*, 762−766.
8. Keating, M. J. (1999) Chronic lymphocytic leukemia, *Semin. Oncol. 26*, 107−114.
9. Morgan, C. J., Gelfand, M., Atreya, C., and Miranker, A. D. (2001) Kidney dialysis-associated amyloidosis: a molecular role for copper in fiber formation, *J. Mol. Biol. 309*, 339−345.
10. Eakin, C. M., Knight, J. D., Morgan, C. J., Gelfand, M. A., and Miranker, A. D. (2002) Formation of a copper specific binding site in non-native states of beta-2-microglobulin, *Biochemistry 41*, 10646−10656.
11. Jobling, M. F., Huang, X., Stewart, L. R., Barnham, K. J., Curtain, C., Volitakis, I., Perugini, M., White, A. R., Cherny, R. A., Masters, C. L., Barrow, C. J., Collins, S. J., Bush, A. I., and Cappai, R. (2001) Copper and zinc binding modulates the aggregation and neurotoxic properties of the prion peptide PrP106−126, *Biochemistry 40*, 8073−8084.
12. Wadsworth, J. D., Hill, A. F., Joiner, S., Jackson, G. S., Clarke, A. R., and Collinge, J. (1999) Strain-specific prion-protein conformation determined by metal ions, *Nat. Cell. Biol. 1*, 55−59.
13. Bush, A. I., and Tanzi, R. E. (2002) The galvanization of beta-amyloid in Alzheimer's disease, *Proc. Natl. Acad. Sci. U.S.A. 99*, 7317−7319.
14. Uversky, V. N., Li, J., and Fink, A. L. (2001) Metal-triggered structural transformations, aggregation, and fibrillation of human alpha-synuclein. A possible molecular NK between Parkinson's disease and heavy metal exposure, *J. Biol. Chem. 276*, 44284−44296.
15. Davis, D. P., Gallo, G., Vogen, S. M., Dul, J. L., Sciarretta, K. L., Kumar, A., Raffen, R., Stevens, F. J., and Argon, Y. (2001) Both the environment and somatic mutations govern the aggregation pathway of pathogenic immunoglobulin light chain, *J. Mol. Biol. 313*, 1021−1034.
16. LeVine, H., 3rd. (1993) Thioflavine T interaction with synthetic Alzheimer's disease beta-amyloid peptides: detection of amyloid aggregation in solution, *Protein Sci. 2*, 404−410.
17. Schuck, P. (2000) Size-distribution analysis of macromolecules by sedimentation velocity ultracentrifugation and lamm equation modeling, *Biophys. J. 78*, 1606−1619.
18. Piotto, M., Saudek, V., and Sklenar, V. (1992) Gradient-tailored excitation for single-quantum NMR spectroscopy of aqueous solutions, *J. Biomol. NMR 2*, 661−665.
19. Lapham, J., Rife, J. P., Moore, P. B., and Crothers, D. M. (1997) Measurement of diffusion constants for nucleic acids by NMR, *J. Biomol. NMR 10*, 255−262.
20. Uversky, V. N. (2002) Natively unfolded proteins: a point where biology waits for physics, *Protein Sci. 11*, 739−756.
21. Kahn, P. C. (1979) The interpretation of near-ultraviolet circular dichroism, *Methods Enzymol. 61*, 339−378.
22. Ubbink, M., Worrall, J. A., Canters, G. W., Groenen, E. J., and Huber, M. (2002) Paramagnetic resonance of biological metal centers, *Annu. Rev. Biophys. Biomol. Struct. 31*, 393−422.
23. Vorbeck-Meister, I., Sommer, R., Vorbeck, F., and Horl, W. H. (1999) Quality of water used for haemodialysis: bacteriological and chemical parameters, *Nephrol. Dial. Transplant. 14*, 666−675.
24. Andrianantoandro, E., Blanchoin, L., Sept, D., McCammon, J. A., and Pollard, T. D. (2001) Kinetic mechanism of end-to-end annealing of actin filaments, *J. Mol. Biol. 312*, 721−730.
25. Rothwell, S. W., Grasser, W. A., and Murphy, D. B. (1986) End-to-end annealing of microtubules in vitro, *J. Cell Biol. 102*, 619−627.
26. Liu, Y., and Eisenberg, D. (2002) 3D domain swapping: as domains continue to swap, *Protein Sci. 11*, 1285−1299.
27. Sinha, N., Tsai, C. J., and Nussinov, R. (2001) A proposed structural model for amyloid fibril elongation: domain swapping forms an interdigitating beta-structure polymer, *Protein Eng. 14*, 93−103.
28. Liu, Y., Gotte, G., Libonati, M., and Eisenberg, D. (2001) A domain-swapped RNase A dimer with implications for amyloid formation, *Nat. Struct. Biol. 8*, 211−214.
29. Cohen, F. E., and Prusiner, S. B. (1998) Pathologic conformations of prion proteins, *Annu. Rev. Biochem. 67*, 793−819.
30. Knaus, K. J., Morillas, M., Swietnicki, W., Malone, M., Surewicz, W. K., and Yee, V. C. (2001) Crystal structure of the human prion protein reveals a mechanism for oligomerization, *Nat. Struct. Biol. 8*, 770−774.
31. Staniforth, R. A., Giannini, S., Higgins, L. D., Conroy, M. J., Hounslow, A. M., Jerala, R., Craven, C. J., and Waltho, J. P. (2001) Three-dimensional domain swapping in the folded and molten-globule states of cystatins, an amyloid-forming structural superfamily, *EMBO J. 20*, 4774−4781.
32. Sanders, A., Jeremy Craven, C., Higgins, L. D., Giannini, S., Conroy, M. J., Hounslow, A. M., Waltho, J. P., and Staniforth, R. A. (2004) Cystatin forms a Tetramer through Structural Rearrangement of Domain-swapped Dimers prior to Amyloidogenesis, *J. Mol. Biol. 336*, 165−178.
33. Jones, S., Smith, D. P., and Radford, S. E. (2003) Role of the N- and C-terminal strands of beta 2-microglobulin in amyloid formation at neutral pH, *J. Mol. Biol. 330*, 935−941.
34. Esposito, G., Michelutti, R., Verdone, G., Viglino, P., Hernandez, H., Robinson, C. V., Amoresano, A., Dal Piaz, F., Monti, M., Pucci, P., Mangione, P., Stoppini, M., Merlini, G., Ferri, G., and Bellotti, V. (2000) Removal of the N-terminal hexapeptide from human beta2-microglobulin facilitates protein aggregation and fibril formation, *Protein Sci. 9*, 831−845.
35. McParland, V. J., Kalverda, A. P., Homans, S. W., and Radford, S. E. (2002) Structural properties of an amyloid precursor of beta-(2)-microglobulin, *Nat. Struct. Biol. 9*, 326−331.
36. Laity, J. H., Lee, B. M., and Wright, P. E. (2001) Zinc finger proteins: new insights into structural and functional diversity, *Curr. Opin. Struct. Biol. 11*, 39−46.
37. Miura, T., Suzuki, K., Kohata, N., and Takeuchi, H. (2000) Metal binding modes of Alzheimer's amyloid beta-peptide in insoluble aggregates and soluble complexes, *Biochemistry 39*, 7024−7031.
38. Aronoff-Spencer, E., Burns, C. S., Avdievich, N. I., Gerfen, G. J., Peisach, J., Antholine, W. E., Ball, H. L., Cohen, F. E., Prusiner, S. B., and Millhauser, G. L. (2000) Identification of the Cu2+ binding sites in the N-terminal domain of the prion protein by EPR and CD spectroscopy, *Biochemistry 39*, 13760−13771.
39. Brown, D. R. (2001) Copper and prion disease, *Brain Res. Bull. 55*, 165−173.

BI049792Q